UNIVERSITY OF CALIFORNIA
SANTA BARBARA

Neural Oscillator Identification via Phase-Locking Behavior

by

Michael J. Schaus

A thesis submitted in partial satisfaction of the
requirements for the degree of
Master of Science

in

Mechanical Engineering

Committee in charge:
Professor Jeff Moehlis, Chair
Professor Francis J. Doyle III
Professor Mustafa Khammash

September 2005

The thesis of Michael J. Schaus is approved:

Professor Francis J. Doyle III

Professor Mustafa Khammash

Professor Jeff Moehlis, Chair

September 2005

Neural Oscillator Identification via Phase-Locking Behavior

Acknowledgments

I would like to first thank my advisor, Professor Jeff Moehlis, for all his guidance through my studies here at UCSB. He clearly remembers what it was like to be a student and was a great help. Also thanks to my committee members, Professors Mustafa Khammash and Frank Doyle, for their insights on improving the final manuscript.

Thanks to my fellow students who helped me with some of the technical and writing issues I encountered—Lina Kim, Barry DeMartini, Sophie Loire, and Erkut Aykutlug.

And of course a special thanks to my family and wonderful girlfriend who helped to make my graduate education both possible and enjoyable.

Abstract

Neural Oscillator Identification via Phase-Locking Behavior

by

Michael J. Schaus

Knowledge of how neurons respond to different types of stimuli could lead to better treatments of diseases such as Parkinson's disease by using deep brain stimulation. This approach involves injecting electrical current into the appropriate region of the brain of a patient in an effort to desynchronize pathologically synchronized groups of neurons which cause the patient to have resting tremors. A neuron's phase response curve (PRC) determines its response to electrical current inputs, and is typically difficult to measure experimentally.

This thesis will show how properties of the PRC can be determined by considering the effects of sinusoidal stimuli on a neuron. Specifically, it will show the relationships between the PRC of a neural oscillator and its phase-locking regions. Knowledge of the PRC can be used to generate good predictions for some of the phase-locking regions of an oscillator, and the phase-locking regions can be used to get some information about the PRC. In the case of Type I neurons where the PRC is always positive, data from the 1:1 locking region can lead to a very good approximation of the PRC. For Type II neurons where the PRC has

both positive and negative portions, data from the locking regions can be used to find combinations of the Fourier coefficients of the PRC which can be used as constraints in fitting procedures that generate Fourier coefficients of the PRC from experimental data. For Type II neurons we can also give a good estimate of the minimum frequency at which periodic behavior will be observed. A detailed method to extract this information from neural systems is provided.

Despite the emphasis on neuroscience, the results are also expected to be applicable to circadian rhythms, where a person's wake-sleep cycles become entrained to the light-dark cycles of the sun. The analysis here could be used to discover more about the PRC and entrainment regions of the system, useful, e.g., in timing the administration of drugs and improving safety of late-shift workers.

Contents

List of Figures

List of Tables

Chapter 1

Introduction

For some neurodegenerative diseases such as Parkinson's disease, symptoms include trembling of a patient's hands which can be associated with waves of electrical activity in the brain [10, 21]. These waves correspond to large groups of neurons firing in synchrony. Current theories suggest that if these neurons can be desynchronized it would alleviate some of the symptoms of the disease, and in fact, there is already an FDA-approved treatment for Parkinson's disease based on this idea called deep brain stimulation [2, 3, 28, 29]. With this treatment, an electrode is implanted into the motor-control region of the brain, injecting a series of high-frequency electrical pulses. This method desynchronizes the neurons to a certain extent, but an understanding how neurons respond to such a stimulus could improve its effectiveness. In this thesis, the focus is on the response of a single neuron to stimuli; population-level response is deferred to future work.

The way a neuron responds to stimuli is characterized by its phase response curve (PRC). The PRC measures how a neuron will respond to an impulsive perturbation depending on at what point the neuron is in its firing cycle. However, knowing the PRC of a neuron allows one to numerically determine the response for any weak stimulus, not just impulsive ones [5, 13]. For simple PRCs and stimuli, it is possible to say quite a bit about the response properties, such as analytical expressions for how a population of oscillators responds to a step-stimulus [5, 6], or how weakly-coupled oscillators can spontaneously synchronize [4, 27].

However, determining the PRC of a neuron is usually not an easy task. One 'obvious' experimental method would give a neuron impulsive kicks of electrical current at different times in its cycle and each time measure the effect on when the neuron spikes next. This has traditionally led to data with too much noise to accurately determine the PRC. Methods that use least-squares fitting techniques of this noisy data to determine the Fourier coefficients of the PRC have been recently proposed in [9, 15]. In the case of [15], random noise inputs are injected into the neuron instead of impulses. Alternatively, if equations are known for the neural system of interest, one can solve the associated adjoint equations to get the PRC [5, 8]. If it is known that the system is in proximity to its bifurcation to periodicity, one can use normal-form theory to at least get the form of the PRC [5].

In this thesis, we propose a new method for determining the properties of

the PRC. A neuron can be reduced to its phase description, where one variable describes its state. In this form, the natural frequency, PRC, and input to the system fully determine the dynamics, but due to the nature of the ODE it cannot be solved using standard analytical techniques. However, assuming that the system is sinusoidally forced, the solution can be approximated by averaging over the forcing cycles. This averaged solution leads to a relationship between the strength of forcing and deviation of the forcing from the neuron's natural frequency where the system stays at a constant phase difference from the forcing—an approximation of the phase-locking boundaries. Data points from the boundaries of the phase-locking regions of neurons subjected to sinusoidal forcing can be fit to this relationship, determining parameters that in some cases lead to a very good approximation of the PRC. In other cases, it can provide constraints on the fitting procedures described in [9, 15]. Additionally, if the PRC is known ahead of time, this relationship allows for very accurate predictions of some of the phase-locking boundaries to be made.

Although our focus is on neural systems, it is expected that the results can also be applied to the study of circadian rhythms. Humans have a natural sleep-wake cycle different from 24 hours, but due to the light-dark cycles of the sun, we are entrained to be on a 24-hour cycle. The scientific community is motivated to study circadian rhythms to administer medication at more effective times [25], develop treatments for jet lag or other sleep disorders, improve safety for late-shift

workers, and improve efficiency of crews on submarines [26]. The techniques in this thesis could help to clarify the properties of this entrainment and the PRC for circadian rhythms.

Chapter 2

Phase equations for nonlinear oscillators

2.1 Neuron modeling

Neurons are the fundamental processing and information carrying units of the central nervous system, involved with sensory, cognitive, regulatory, motor, and other functions. In the human brain there are estimated to be 10^{11} of these interconnected cells [16]. To create a mathematical model of a neuron, one looks at how they are put together. Their outer membrane is made of a lipid bilayer which acts as an electrical capacitor. Piercing through this are proteins that control the flow of ions through the membrane; such gating proteins act as nonlinear resistors. The potential difference between the inside and outside of the neuron drives the

states of the corresponding gating proteins. Finally, ion pumps maintain the differences in ion concentrations inside and outside of the membrane and behave as batteries. Putting these components together appropriately and applying circuit laws results in a *conductance-based* neuron model [7, 16]. This thesis considers the dynamics of reductions of such conductance-based models subject to sinusoidal current stimuli in the case that they have an attracting limit cycle in the absence of such stimulus.

2.2 Phase reduction

Nonlinear oscillators with attracting limit cycles can have the limit cycle mapped to phase coordinates to simplify further analysis, as detailed below [5, 11, 31, 32]. Here we consider a nonlinear oscillator described by a generic conductance-based model of a single neuron,

$$C\dot{V} = I_g(V, \mathbf{n}) + I_b, \tag{2.1}$$

$$\dot{\mathbf{n}} = \mathbf{N}(V, \mathbf{n}), \tag{2.2}$$

with $(V, \mathbf{n})^T \in \mathbb{R}^N$. V is the voltage across the membrane of the neuron, $\mathbf{n}$ is the (N-1)-dimension vector of gating variables (which determine the states of the ion channels in the model), and C is the membrane capacitance. $I_g(V, \mathbf{n})$ is the vector of membrane currents and I_b is the baseline current that sets the natural frequency of the oscillator. Examples of such models include the Hodgkin-Huxley equations

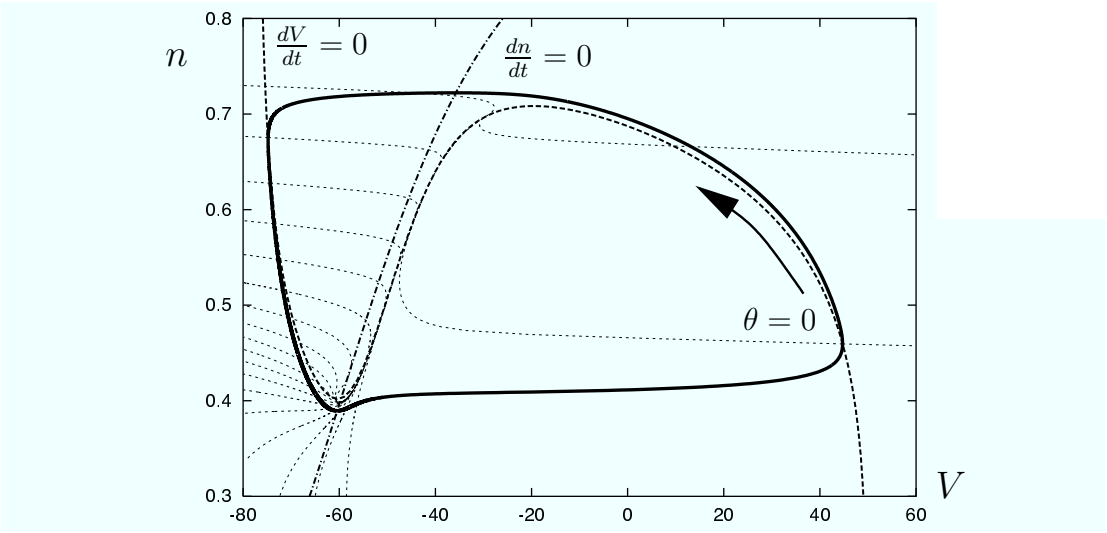

Figure 2.1: The phase-space for a two-dimensional reduction of the Hodgkin-Huxley neuron model with $I_b = 10$. The limit cycle is in bold while the isochrons, equally spaced in time, are dotted. The thicker dotted lines are the nullclines of the system, where $d(\cdot)/dt = 0$.

(HH) [14, 23] and the Hindmarsh-Rose equations (HR) [24]; see Appendix A. It will prove useful to rewrite Equations (2.1) and (2.2) in the general form

$$\frac{d\mathbf{X}}{dt} = \mathbf{F}(\mathbf{X}), \tag{2.3}$$

where $\mathbf{X} = (V, \mathbf{n})^T \in \mathbb{R}^N$ and $\mathbf{F}(\mathbf{X})$ is the baseline vector field. We suppose that this system has an attracting limit cycle $\mathbf{X}_0(t)$ with period $2\pi/\omega$.

To move to phase coordinates, we introduce the scalar phase variable $\theta(\mathbf{X}) \in [0, 2\pi)$ for all $\mathbf{X}$ in $\mathcal{U}$, some neighborhood of $\mathbf{X}_0$ contained within its basin of attraction, such that the evolution of the phase takes the form

$$\frac{d\theta(\mathbf{X})}{dt} = \omega \tag{2.4}$$

for all $\mathbf{X} \in \mathcal{U}$. That is, θ evolves linearly in time. This is accomplished by defining the level sets of $\theta(\mathbf{X})$, called *isochrons*, as follows. Let $\mathbf{X}_0^S$ be the point on the limit

cycle with the highest voltage, i.e. where the neuron spikes. We define $\theta(\mathbf{X}_0^S) = 0$. To determine θ for the rest of the points on the limit cycle (e.g. $\mathbf{X}_0^P$), let the system evolve from $\mathbf{X}_0^S$ with $\theta(\mathbf{X}_0^P) = \omega t$. This method assigns a value of θ in $[0, 2\pi)$ to every point on $\mathbf{X}_0$. The isochron associated with a point $\mathbf{X}_0^P$ on $\mathbf{X}_0$ is defined as the set of all initial conditions, $\mathbf{X} \in \mathcal{U}$, such that the distance (evaluated at time t) between trajectories starting at $\mathbf{X}_0^P$ and $\mathbf{X}$ goes to zero as $t \to \infty$. The point $\mathbf{X}_0^P$ and the points on its isochron, $\mathbf{X}_{iso}^P$, are said to have the same aymptotic phase. As in Figure 2.1, it is useful to plot isochrons equally spaced in time so that a sense of the flow on the limit cycle can be gained. This figure shows results for a two-dimensional reduction of the HH equations given by Equations (4.35) and (4.36) of [17].

Now, consider the system

$$\frac{d\mathbf{X}}{dt} = \mathbf{F}(\mathbf{X}) + \epsilon \mathbf{G}(\mathbf{X}, t), \tag{2.5}$$

where $\epsilon \mathbf{G}(\mathbf{X}, t)$ is a small perturbation to the system. Using the chain rule and Equation (2.4) which tells us that $d\theta/dt = \omega$ in the absence of perturbations,

$$\frac{d\theta}{dt} = \frac{\partial \theta}{\partial \mathbf{X}} \cdot \frac{d\mathbf{X}}{dt} = \frac{\partial \theta}{\partial \mathbf{X}} \cdot (\mathbf{F}(\mathbf{X}) + \epsilon \mathbf{G}(\mathbf{X}, t)) = \omega + \epsilon \frac{\partial \theta}{\partial \mathbf{X}} \cdot \mathbf{G}(\mathbf{X}, t). \tag{2.6}$$

Defining the *phase response curve* (PRC, discussed in more depth in Section 2.3) as

$$\mathbf{Z}(\theta) = \left. \frac{\partial \theta}{\partial \mathbf{X}} \right|_{\mathbf{X}_0(\theta)}, \tag{2.7}$$

an approximation to Equation (2.5) is given by

$$\frac{d\theta}{dt} = \omega + \mathbf{Z}(\theta) \cdot \epsilon \mathbf{G}(\mathbf{X}_0, t). \tag{2.8}$$

Suppose now that $\epsilon\mathbf{G} = \epsilon\mathbf{G}(t) = (I(t), \mathbf{0})$, where $I(t)$ is a current stimulus that directly affects only the voltage of the neuron. (If reversal potentials were included, $I(t)$ would be replaced by $I(V, t)$.) Including C so that the units work out correctly and using only the voltage component of $\mathbf{Z}(\theta)$, the general form for the phase reduced neural oscillator becomes

$$\frac{d\theta}{dt} = \omega + \frac{Z(\theta)}{C} I(t). \tag{2.9}$$

The phase response curve can be written as

$$Z(\theta) = C Z_d \zeta(\theta), \tag{2.10}$$

where Z_d is a dimensional constant (units of $rad/coulomb$), and $\zeta(\theta)$ is a non-dimensional $\mathcal{O}(1)$ function. For this thesis, the injected current is sinusoidal with the form

$$I(t) = I_f \sin(\omega_f t), \tag{2.11}$$

where I_f is the strength of the injected current in milliamperes and ω_f is the frequency of the forcing.

2.3 Phase response curves

The phase response curve (PRC) of a system determines how small perturbations in a given variable affect the system's phase. By definition, the PRC

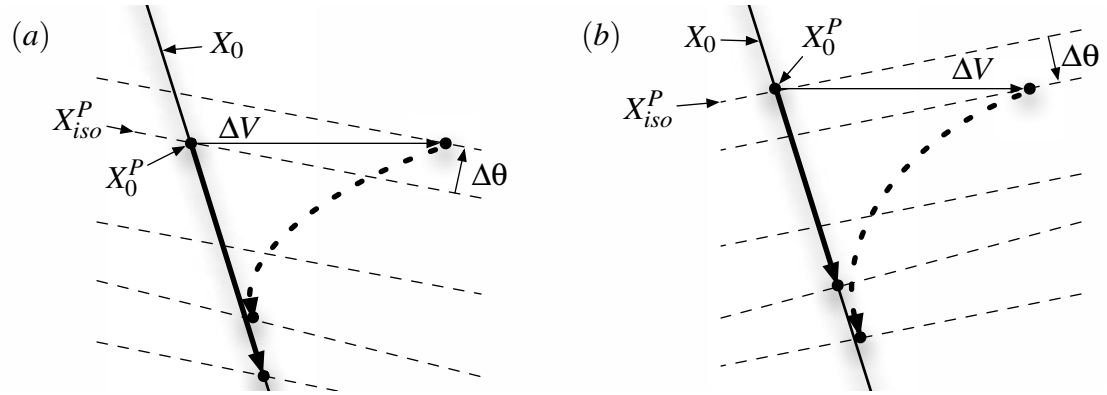

Figure 2.2: Typical details of isochrons (equally spaced in time) for a neuron model. The spacing and orientation of the isochrons determines how much a voltage perturbation will advance or push back the phase. (a) Perturbations in voltage lead to a decrease in the phase of the system. (b) Perturbations result in an increase in phase.

characterizes response only to impulsive perturbations. The PRC does not describe the response for different frequencies of an input, such as a Bode Plot would, but rather how the response depends on what point during the cycle of the oscillator an impulse is applied. When the PRC is positive (resp., negative), positive perturbations increase (resp., decrease) the phase. This behavior, closely related to the system's isochrons, is detailed in Figure 2.2. For neural oscillators such as in this thesis, a useful way to think about the PRC is

$$Z(\theta) = \frac{\partial \theta}{\partial V} = \lim_{\Delta V \to 0} \frac{\Delta \theta}{\Delta V}, \tag{2.12}$$

with units rad/mV.

The PRC for the HH system with $I_b = 10$ is shown in Figure 2.3. This was found by numerically solving an associated adjoint equation, as implemented in the computer program XPP [5, 8]. PRCs in general are not required to be zero at values of 0 and 2π. That this occurs here can be understood by recognizing that

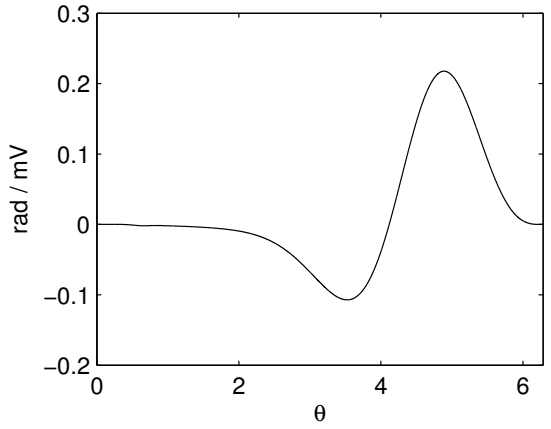

Figure 2.3: Phase response curve for the HH system with baseline current $I_b = 10$. Isochrons for the part of the system where the PRC is negative look similar to Figure 2.2(a). Isochrons where the PRC is positive look similar to Figure 2.2(b).

HH is an example of a *fast-slow* system. When the two-dimensional phase-space is drawn (as has been done Figure 2.1), voltage is considered to be a 'fast' variable and the gating variable n is considered to be 'slow'. Looking at the isochrons near where the neuron spikes, we see that they are sparsely spaced (due to the small amount of time spent in that part of phase-space) and almost parallel to the V-axis. Thus, a voltage impulse would not push the system onto a significantly different isochron and the value of the PRC is almost zero. In other parts of phase-space where the isochrons are closer together and more 'steep' compared to the V-axis, the PRC takes on a larger magnitude. Note that the slope of the isochrons (along with the general direction of the flow) determines whether the PRC is positive or negative at that point, as in Figure 2.2.

Nullcline analysis can be used with fast-slow systems to approximately determine the shape (and existence) of the limit cycle. A nullcline of a state-variable

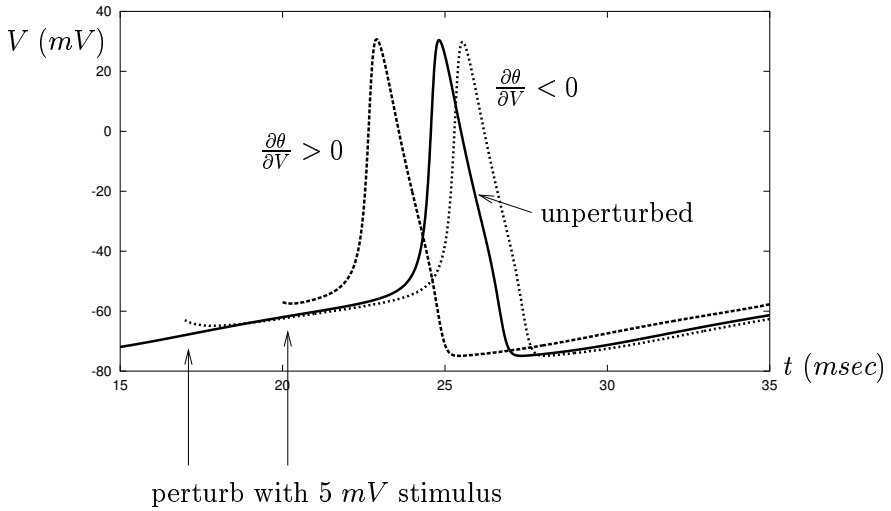

Figure 2.4: Effect of impulsive perturbations on an HH neuron. Impulses at different points, indicated by the vertical arrows, correspond to different signs of the PRC and thus either accelerate or delay the onset of the next spike. The solid line is the unperturbed voltage trace.

in a system is defined as the curve where the time-derivative of that state-variable is zero. The intersections of all the system's nullclines make up the system's fixed points. In Figure 2.1 it can be seen that the limit cycle of the (reduced) HH system spends much of its time near the V-nullcline. There is one intersection of the nullclines which corresponds to an unstable fixed point. Near this fixed point the isochrons are the most tightly spaced of anywhere else in the system, indicating that the system spends most of its time on the portion of the limit cycle near the fixed point.

A sample voltage trace for the HH system can be seen in Figure 2.4. Voltage perturbations are applied to the neuron at different points during its refractory period, corresponding to phases with opposite signs of the PRC. Thus, it is clearly seen that the exact timing of a voltage perturbation in a neuron has an important

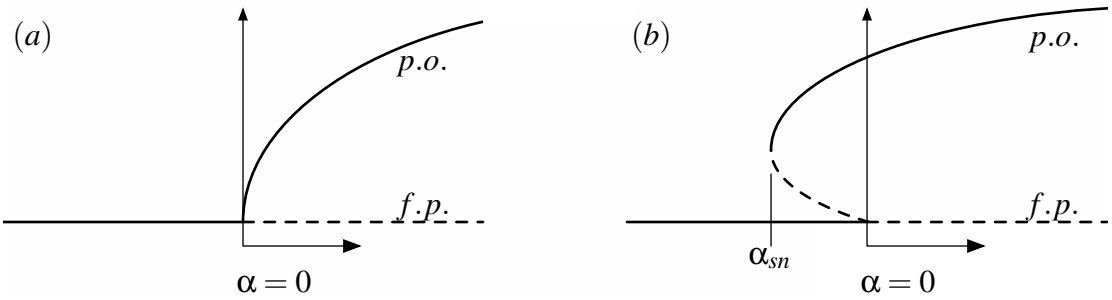

Figure 2.5: (a) Supercritical Hopf bifurcation. (b) Bautin (subcritical Hopf at $\alpha = 0$, saddle node bifurcation of periodic orbits at $\alpha = \alpha_{sn}$) bifurcation. Here, the bifurcation parameter is α and the periodic orbits arise at $\alpha = 0$. The vertical axis represents the size of the periodic orbit. The periodic orbit (p.o.) and fixed point (f.p.) branches are as shown. Solid segments are stable, dashed segments are unstable. Phase-space representations can be seen in Figure 2.6.

effect on its overall dynamics. To measure the PRC of a neuron, experiments can be done very similar to what is seen in Figure 2.4—measure $\Delta\theta/\Delta V$ directly by injecting an impulse at a given phase and seeing how this impulse affects the arrival of the next spike. However, such experiments are difficult to set up and in general result in data with too much noise to be very useful. Hence, an improvement upon this method is explored in this thesis.

2.4 Bifurcations to periodicity

For a generic vector field, there are four codimension one bifurcations that can give rise to a limit cycle [12]. These are SNIPER (saddle node of fixed points on a periodic orbit), supercritical Hopf (a stable fixed point becomes unstable and a stable periodic orbit is formed—see Figure 2.5(a)), Bautin (which includes a subcritical Hopf and a saddle node bifurcation of periodic orbits—see Figure 2.5(b)),

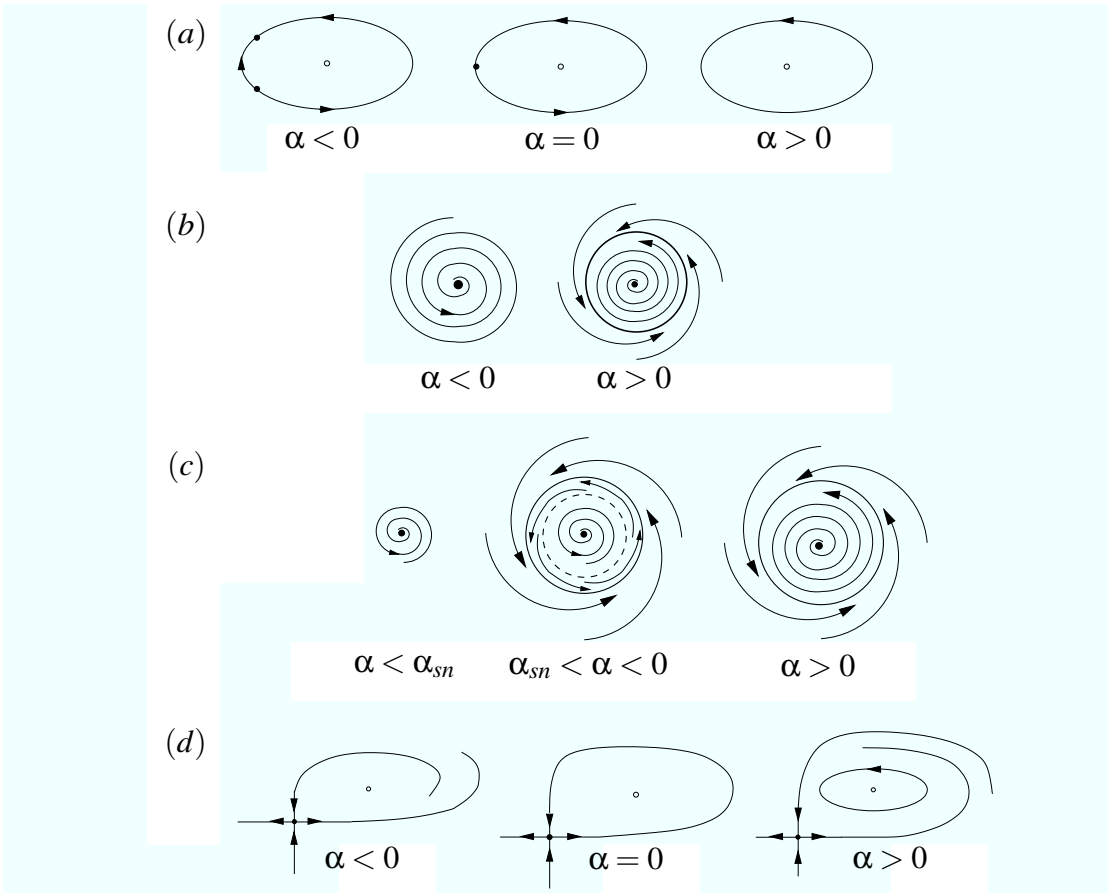

Figure 2.6: The four codimension one bifurcations to periodicity. The primary bifurcations occur at $\alpha = 0$. (a) SNIPER. (b) Supercritical Hopf (as in Figure 2.5(a)). (c) Bautin (subcritical Hopf at $\alpha = 0$, saddle node bifurcation of periodic orbits at $\alpha = \alpha_{sn}$ as in Figure 2.5(b)). Here, the solid (resp., dashed) closed curve represents a stable (resp., unstable) periodic orbit. (d) Homoclinic. Figure adapted from [5].

and homoclinic (a homoclinic orbit to a hyperbolic saddle node exists at the bifurcation point) bifurcations. Figure 2.6 shows how the phase-space of the systems characterized by these bifurcations changes as the bifurcation parameter passes through the bifurcation point $\alpha = 0$.

Neuron models have been developed which undergo each of these four codimension one bifurcations to periodic firing. The Hindmarsh-Rose system has a

SNIPER bifurcation, Hodgkin-Huxley has Bautin (more accurately, a bifurcation diagram that closely resembles Bautin), Fitzhugh-Nagumo can have a supercritical Hopf, and Morris-Lecar has a homoclinic bifurcation [5]. For these neuron models the bifurcation parameter is the baseline injected current, I_b.

In this thesis, we focus on the Hodgkin-Huxley (HH) and Hindmarsh-Rose (HR) neurons, which represent typical examples of the two most common types of neurons. HR neurons are called Type I because their PRC is always positive. HH neurons are Type II because their PRCs are both negative and positive. Again, due to the fast-slow nature of the models, both PRCs are approximately zero at $\theta = 0, 2\pi$.

2.5 Phase-locking behavior

Phase-locking occurs when a system's response cycles at either the forcing frequency or a ratio of the forcing frequency determined by both the strength of the forcing and how far from its natural frequency the system is being forced. When this happens, the system is said to be *entrained* to the forcing. The phase-locking regions shown in Figure 2.7 (and, e.g. Figures 3.2 and 3.4) are called Arnold Tongues [22, 30], or more simply tongues or wedges. Inside these tongues, forcing cycles and resulting forced oscillations have frequencies in specific ratios. In general, $n : m$ phase-locking refers to n cycles of forcing resulting in m cycles of system oscillation. It is also useful to define the ratio $\rho = m/n$, called the

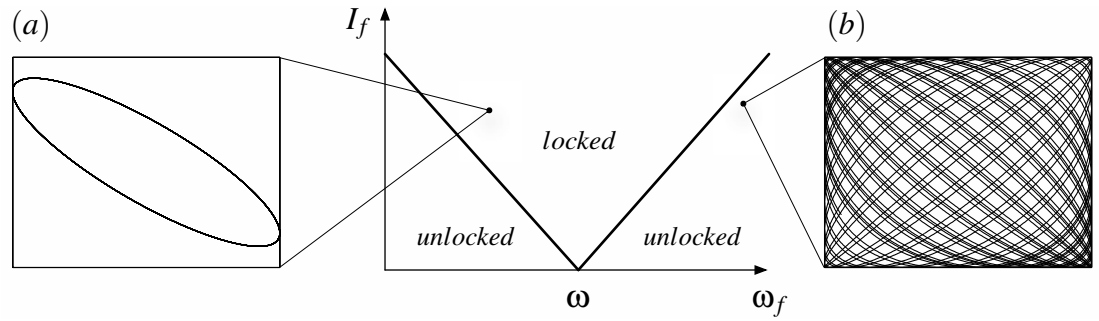

Figure 2.7: Sketch of the 1:1 phase-locking boundary for a neural oscillator. Associated with the two types of regions are Lissajous plots at typical points, where one axis plots the amplitude of the forcing function while the other axis plots the amplitude of the system response. (a) Synchronous state—the oscillatory periods of the forcing function and the system response are equal, forming a closed curve. (b) Quasiperiodic state—the ratio of the two periods is irrational. No point on the plot is ever returned to, eventually causing the entire region to become filled.

rotation number [22].

As seen in Figure 2.7, when $\omega_f = \omega$ (i.e. the forcing frequency equals the oscillator's natural frequency), the system is phase-locked for even an infinitesimal strength of forcing, I_f. In this case the forcing is not really entraining the system; they are phase-locked by definition of having no change in relative phase. When $\omega_f \neq \omega$, there are competing effects leading to two qualitatively different regimes in the $\omega_f - I_f$ space. The oscillator would like to persist at its natural frequency, but the forcing is trying to make it oscillate at a different frequency. If the forcing is strong enough, it becomes phase-locked and, if in the 1:1 tongue, the system fires at the forcing frequency. If inside a different tongue the system fires at $\rho\omega_f$. These are called *synchronous* states. When the system is outside of the Arnold tongues, phase-locking does not occur, corresponding to an irrational rotation number. This type of response is called *quasiperiodic*.

In theory, $n : m$ tongues exist for all $n, m \in \mathbb{N}$, but in real systems the vast majority have widths too small to measure [30]. In general, the larger the values of n or m, the thinner the tongue will be. More on the existence and behavior of higher-order tongues can be found by exploring Farey trees [19], Cantor sets [20], and the Devil's staircase [1, 18, 20].

Chapter 3

Universal entrainment curves for sinusoidal forcing

3.1 Introduction

In this chapter, it is assumed that the PRC $Z(\theta)$ is known. This could be from the proximity of the neural system to a bifurcation which gives rise to its periodicity [5], from the numerical solution to the adjoint equations for the neural model of interest [5, 8], or from recently proposed least-squares fitting procedures which can be applied to experimental data [9, 15]. We will show how such knowledge of $Z(\theta)$ can be used to find an analytical approximation for the boundaries of phase-locked regimes. Near bifurcations to periodicity, we call such boundaries *universal entrainment curves*.

3.2 Non-dimensionalization of the phase equations

Non-dimensionalizing the phase-reduced equations allows them to be studied without worrying about individual parameter values or scales, such as an oscillator's natural frequency. General trends can be seen which can be applied to specific oscillators by computing the actual value of the non-dimensional parameters.

Let the non-dimensionalized time be

$$\tau = \omega_f t, \tag{3.1}$$

where ω_f is the frequency at which the oscillator is forced. The time derivative is transformed as

$$\frac{d}{dt} = \omega_f \frac{d}{d\tau}. \tag{3.2}$$

Using these transformations, the non-dimensionalized version of Equation (2.9) is

$$\frac{d\theta}{d\tau} = \frac{\omega}{\omega_f} + \frac{I_f Z_d}{\omega_f}\zeta(\theta)\sin\tau. \tag{3.3}$$

We can then define the two non-dimensional quantities

$$\lambda = \frac{\omega_f}{\omega} \tag{3.4}$$

$$\mu = \frac{I_f Z_d}{\omega_f} \tag{3.5}$$

for easier plotting and conceptual understanding. λ is the ratio between the forcing and natural frequencies, while μ measures the strength of the forcing.

This simplifies Equation (3.3) to

$$\frac{d\theta}{d\tau} = \frac{1}{\lambda} + \mu\zeta(\theta)\sin\tau. \tag{3.6}$$

3.3 Averaging the phase equations

The solution $\theta(\tau)$ cannot be found explicitly from Equation (3.6) through standard ODE techniques such as separation of variables. However, through averaging the equations, a close approximation to the solution can be found. We will show that averaging also allows approximations of phase-locking boundaries to be found, with their form being related to the type of bifurcation that gives rise to periodic firing for the neuron.

Consider that the system is forced with frequency $\omega_f \approx \frac{q}{p}\omega$, i.e.

$$\frac{\omega}{\omega_f} = \frac{p}{q} + \epsilon\Delta, \tag{3.7}$$

where p and q are relatively prime integers and $\epsilon\Delta$ represents a small detuning with respect to the center of the $q : p$ phase-locking region. The system is put into a rotating reference frame by letting

$$\gamma = \theta - \frac{p}{q}\tau, \tag{3.8}$$

where γ is the difference in phase angle between the original system and the forcing, adjusted for proximity to the $q : p$ tongue. The time-derivative is then

$$\frac{d\gamma}{d\tau} = \frac{d\theta}{d\tau} - \frac{p}{q}. \tag{3.9}$$

These transform Equation (3.6) into

$$\frac{d\gamma}{d\tau} = \epsilon\Delta + \mu\zeta\left(\gamma + \frac{p}{q}\tau\right)\sin\tau. \tag{3.10}$$

We can then define

$$\epsilon\tilde{I_f} = I_f \tag{3.11}$$

$$\epsilon\kappa = \epsilon\frac{\tilde{I_f}Z_d}{\omega_f} = \mu, \tag{3.12}$$

where ϵ is small, $\tilde{I_f}$ is an $\mathcal{O}(1)$ amount of current, and $\epsilon\kappa$ measures the strength of the forcing. Note that ϵ, Δ, and κ are dimensionless. These transform Equation (3.10) into

$$\frac{d\gamma}{d\tau} = \epsilon\left[\Delta + \kappa\zeta\left(\gamma + \frac{p}{q}\tau\right)\sin\tau\right]. \tag{3.13}$$

Using the averaging theorem (Theorem 4.1 of [12]) and introducing the averaged variable $\bar{\gamma}$,

$$\frac{d\bar{\gamma}}{d\tau} = \frac{\epsilon}{2\pi q}\int_0^{2\pi q}\left[\Delta + \kappa\zeta\left(\bar{\gamma} + \frac{p}{q}\tau\right)\sin\tau\right]d\tau \tag{3.14}$$

$$= \epsilon\left\{\Delta + \frac{\kappa}{2\pi q}\int_0^{2\pi q}\left[\zeta\left(\bar{\gamma} + \frac{p}{q}\tau\right)\sin\tau\right]d\tau\right\}. \tag{3.15}$$

The averaging theorem states that solutions to Equation (3.14) remain within $\mathcal{O}(\epsilon)$ of solutions to Equation (3.13) (i.e. $\gamma = \bar{\gamma} + \mathcal{O}(\epsilon)$) for times of $\mathcal{O}(1/\epsilon)$. Furthermore, fixed points of Equation (3.14) (i.e. values of $\bar{\gamma}$ where $d\bar{\gamma}/d\tau = 0$) correspond to the periodic orbits of Equation (3.13). The integration period of $2\pi q$ was chosen because it is the smallest common multiple of the periods in the

Table 3.1: Forms of the phase response curves for the four codimension one bifurcations to periodicity. $Z(\theta)$ comes from analysis of the normal forms of the bifurcations as done in [5].

Bifurcation	$Z(\theta)$	μ	$\zeta(\theta)$	$g(\bar{\gamma})$
SNIPER	$\frac{c_{sn}}{\omega}(1-\cos\theta)$	$\frac{I_f c_{sn}}{\omega_f \omega C}$	$1-\cos\theta$	$-\frac{\kappa}{2}\sin\bar{\gamma}$
Bautin	$\frac{\lvert c_B\rvert}{\lvert\omega-\omega_{SN}\rvert}\sin(\theta-\phi_B)$	$\frac{I_f\lvert c_B\rvert}{\omega_f\lvert\omega-\omega_{SN}\rvert C}$	$\sin(\theta-\phi_B)$	$\frac{\kappa}{2}\cos\bar{\gamma}$
Hopf	$\frac{\lvert c_H\rvert}{\sqrt{\lvert\omega-\omega_H\rvert}}\sin(\theta-\phi_H)$	$\frac{I_f\lvert c_H\rvert}{\omega_f\sqrt{\lvert\omega-\omega_H\rvert}C}$	$\sin(\theta-\phi_H)$	$\frac{\kappa}{2}\cos\bar{\gamma}$
Homoclinic	$c_{hc}\omega e^{(2\pi l_u/\omega)}e^{(-l_u\theta/\omega)}$			

integrand. We can then define the function

$$g(\bar{\gamma}) = \frac{\kappa}{2\pi q}\int_0^{2\pi q}\left[\zeta\left(\bar{\gamma}+\frac{p}{q}\tau\right)\sin\tau\right]d\tau. \tag{3.16}$$

Using these results, Table 3.1 shows the forms of $Z(\theta)$, μ, $\zeta(\theta)$, and $g(\bar{\gamma})$ for the bifurcation types discussed in detail in this thesis. Only $Z(\theta)$ is shown for homoclinic neurons; due to their uncommon nature and significant difference in necessary analysis, neurons exhibiting homoclinic bifurcations will not be considered in the remainder of this thesis.

Computing $g(\bar{\gamma})$ for anything but the most simple PRCs gets difficult very quickly. To alleviate this problem, the PRC can be expanded as a Fourier series,

$$\zeta\left(\bar{\gamma}+\frac{p}{q}\tau\right) = \sum_{j=0}^{\infty}\left[a_j\cos\left(j\bar{\gamma}+j\frac{p}{q}\tau\right)\right] + \sum_{j=1}^{\infty}\left[b_j\sin\left(j\bar{\gamma}+j\frac{p}{q}\tau\right)\right]. \tag{3.17}$$

The relationship between the coefficients in this series, e.g. a_j, and coefficients derived from the original PRC (with units rad/mV), e.g. a_j^{PRC}, is

$$a_j = a_j^{PRC}\frac{1}{CZ_d}, \tag{3.18}$$

which comes from Equation (2.10). For the terms in the series to contribute a non-zero value to the integral in Equation (3.16) when being multiplied by $\sin\tau$,

the sin term and the ζ term must have the same frequency. Thus, we must have $j\frac{p}{q} = 1$. Since $j = \frac{q}{p}$ must be an integer, this method of averaging only gives nontrivial results for $n:1$ tongues. For other tongues, a higher-order averaging technique might provide better results. Taking this into account, $g(\bar{\gamma})$ can be written as

$$g(\bar{\gamma}) = \frac{\kappa}{2\pi q}\int_0^{2\pi q}\left[a_{q/p}\cos\left(\frac{q}{p}\bar{\gamma}+\tau\right)\sin\tau + b_{q/p}\sin\left(\frac{q}{p}\bar{\gamma}+\tau\right)\sin\tau\right]d\tau, \quad (3.19)$$

which evaluates to

$$g(\bar{\gamma}) = \frac{\kappa}{2}\left[-a_{q/p}\sin\left(\frac{q}{p}\bar{\gamma}\right) + b_{q/p}\cos\left(\frac{q}{p}\bar{\gamma}\right)\right]. \quad (3.20)$$

Combining the sin and cos terms from Equation (3.20) to a single sin term with a phase lag turns Equation (3.14) into

$$\frac{d\bar{\gamma}}{d\tau} = \epsilon\Delta + \frac{\epsilon\kappa}{2}\sqrt{a_{q/p}^2 + b_{q/p}^2}\sin\left(\frac{q}{p}\bar{\gamma} - \tan^{-1}\frac{b_{q/p}}{a_{q/p}}\right). \quad (3.21)$$

3.4 SNIPER PRC

For $Z(\theta) \sim (1-\cos\theta)$, corresponding to proximity to a SNIPER bifurcation, Equation (3.16) is nonzero only when $p/q = 1$. Equation (3.14) evaluates to

$$\frac{d\bar{\gamma}}{d\tau} = \epsilon\left(\Delta - \frac{\kappa}{2}\sin\bar{\gamma}\right). \quad (3.22)$$

Thus, as shown in Figure 3.1, when the detuning is greater than some proportional value of the forcing strength, the plot of $d\bar{\gamma}/d\tau$ versus $\bar{\gamma}$ no long crosses zero and the

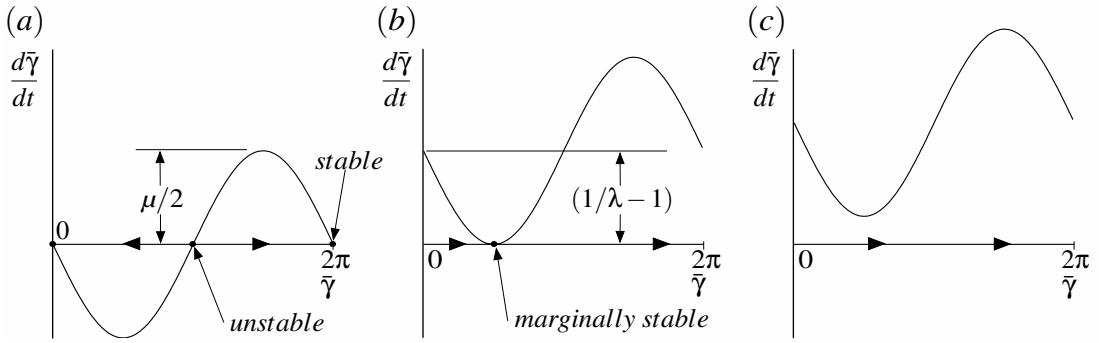

Figure 3.1: $d\bar{\gamma}/d\tau$ versus $\bar{\gamma}$, the averaged solution of the phase equations with a SNIPER bifurcation (similar for Bautin and supercritical Hopf). (a) The detuning $\left(\frac{1}{\lambda} - 1\right) = 0$. (b) $\left(\frac{1}{\lambda} - 1\right) = \frac{\mu}{2}$. (c) $\left(\frac{1}{\lambda} - 1\right) > \frac{\mu}{2}$. Following the arrows, it can be seen that (a) has one stable and one unstable fixed point, (b) has one marginally stable fixed point, and (c) has no fixed points. Note that $\bar{\gamma} = 0$ and $\bar{\gamma} = 2\pi$ correspond to the same point.

difference between the system phase and the forcing phase continually changes—the system is no longer entrained to the forcing. This can be used to produce an approximate analytical boundary between the locked and unlocked region of 1:1 forcing. This boundary is shown in Figure 3.2, and given analytically by

$$\epsilon\Delta = \pm\frac{\epsilon\kappa}{2} \quad \Rightarrow \quad \left(\frac{1}{\lambda} - 1\right) = \pm\frac{\mu}{2}. \tag{3.23}$$

This relationship is representative of what is happening in Figure 3.1(b). Also shown in Figure 3.2 are the actual phase-locking boundaries for the phase-reduced system. To locate these boundaries, XPP [8] was used to first vary the forcing frequency at a given forcing strength to find points on the boundary on both sides, then following these bifurcations in the two parameters λ and μ. The averaged solution to the 1:1 boundary closely matches the actual boundary for relatively small values of μ.

Certain tongues which exist in other systems were not found in this phase

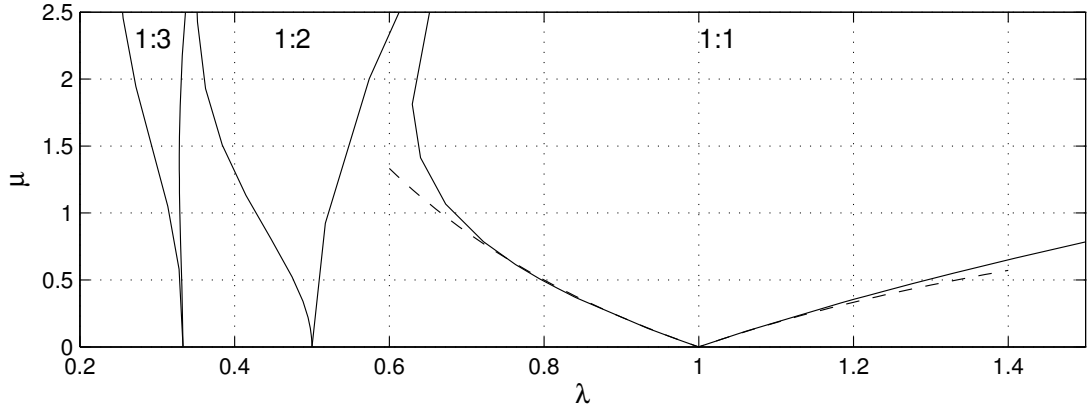

Figure 3.2: Phase-locking regions ('tongues') for the phase-reduced oscillator exhibiting a SNIPER bifurcation. The dotted lines near the 1:1 tongue are from the averaged solution.

reduced model, such as 2:3 and 2:1. It is fully expected not to find the 2:1 tongue because there is no $\sin 2\theta$ or $\cos 2\theta$ (or higher) Fourier component of the PRC, and Equation (3.16) is only nonzero when $p/q = 1$. However, a 1:4 tongue, thinner than the 1:3 tongue, was found. This progression indicates there are likely to exist many more $1 : m$ tongues of continually decreasing thickness. Unfortunately, the method of averaging used in this thesis does not tell us any additional information about such tongues. Outside of the tongues the response was quasiperiodic.

3.5 Bautin and supercritical Hopf PRCs

For $Z(\theta) \sim \sin(\theta - \phi)$, corresponding to proximity to either the Bautin or supercritical Hopf bifurcations, Equation (3.16) is again nonzero only when $p/q =$

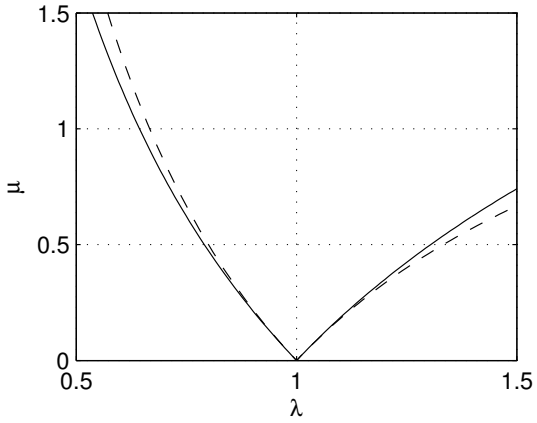

Figure 3.3: 1:1 phase-locking region for the phase-reduced oscillator exhibiting a supercritical Hopf or Bautin bifurcation. Dotted lines: averaged boundary. Solid lines: actual boundary.

1. Equation (3.14) evaluates to

$$\frac{d\bar{\gamma}}{d\tau} = \epsilon \left(\Delta + \frac{\kappa}{2} \cos \bar{\gamma} \right). \tag{3.24}$$

The plot of $d\bar{\gamma}/d\tau$ versus $\bar{\gamma}$ is qualitatively the same as for the SNIPER bifurcation shown in Figure 3.1. The analytical phase-locking boundary for both supercritical Hopf and Bautin is again given by Equation (3.23), recalling that the definition of μ depends on the bifurcation (see Table 3.1). Figure 3.3 shows the analytical and actual boundaries for these two bifurcations. Using XPP, only the 1:1 tongue could be reliably found for the unaveraged Equation (3.6). Again, it is expected that there be no 2:1 or greater whole-number ratio tongue because the PRC has no contribution to the Fourier series beyond $\sin \theta$. We were unable to locate tongues with ratios smaller than 1:1 (such as 1:2).

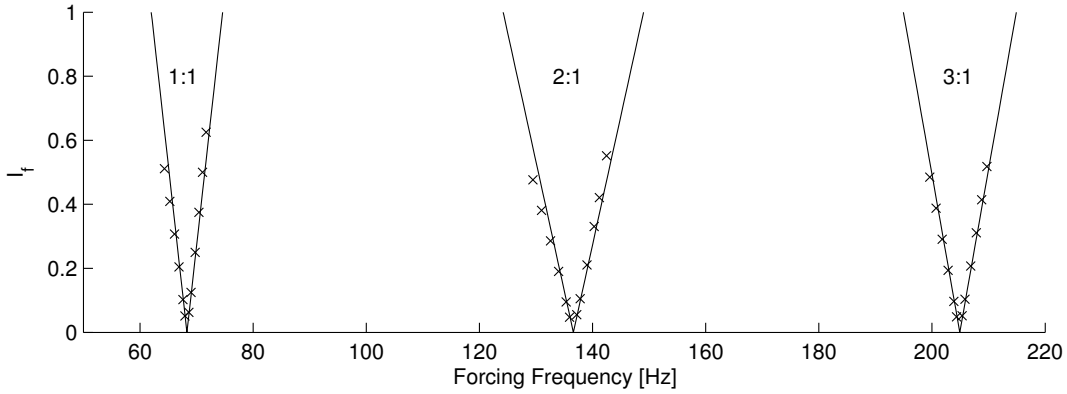

Figure 3.4: The lines show predicted phase-locking boundaries for the HH system with $I_b = 10$. The data points come from numerically finding the actual boundaries.

3.6 General PRCs

For the general case where $Z(\theta)$ is represented by a Fourier series, $d\bar{\gamma}/dt$ is given by Equation (3.21). The tongues are thus approximately

$$\left(\frac{1}{\lambda} - \frac{p}{q}\right) = \pm\frac{\mu}{2}\sqrt{a_{q/p}^2 + b_{q/p}^2}, \tag{3.25}$$

recalling that q/p must be an integer. Rewriting with dimensional terms,

$$\left(\frac{\omega}{\omega_f} - \frac{p}{q}\right) = \pm\frac{I_f}{2\omega_f C}\sqrt{(a_{q/p}^{PRC})^2 + (b_{q/p}^{PRC})^2}. \tag{3.26}$$

Figure 3.4 shows the averaged solution to the whole-number ratio phase-locking regions of the HH system. Also included are actual points from these boundaries found numerically (details of how this was done are included in Appendix B.1). The plot shows that by knowing the PRC of a system, some of the phase-locking regions can be accurately predicted. Because HH has a bifurcation similar to Bautin, the tendency for the data points to be to the left of the averaged boundaries can be explained by comparing with Figure 3.3.

Chapter 4

Using phase-locking data to deduce properties of the phase response curve

4.1 Introduction

In this chapter, we assume that the PRC $Z(\theta)$ is not known for the system of interest, but we do know if it is of Type I or Type II. We show how data points on the phase-locking boundaries can be used to deduce properties of the PRC. In the case that the system is known to be close to a SNIPER bifurcation, such data can lead to a very good approximation of $Z(\theta)$. In other cases, it provides constraints on recently proposed least-squares fitting procedures for $Z(\theta)$ [9, 15].

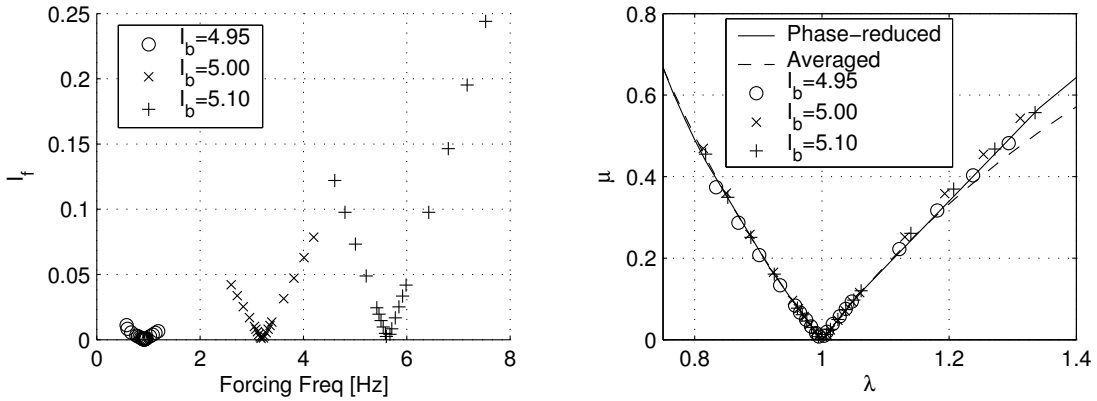

Figure 4.1: Left panel: Raw data taken for phase-locking boundary of the HR system for three values of I_b. Right panel: Same data non-dimensionalized using a value of c_{sn} fitted individually to the SNIPER averaged boundary for each value of I_b.

More details of this process for determining properties of the PRC are included in Appendix B.1.

4.2 SNIPER PRC / Type I

Suppose it is known that a given neuron is of Type I, i.e. it gives rise to its periodic firing though a SNIPER bifurcation and the PRC is always positive. Figure 4.1 shows data on the 1:1 phase-locking boundary for the HR system, a two-dimensional set of equations which exhibits Type I behavior. Data was taken for three different values of the baseline current (I_b = 4.95, 5.00, 5.10), corresponding to three different natural frequencies.

To find the locking regions in these equations, we simulated them with MATLAB, plotting the voltage of the neuron each time the forcing sinusoid reached zero radians (i.e. when it reached the beginning of each cycle), creating a Poincaré

map. After many cycles, if the neuron settled down to a single voltage each time it was strobed, it was considered to be phase-locked with the forcing sinusoid. The closer the forcing frequency was to the actual boundary the longer it took to clearly synchronize, typically requiring between 300–600 cycles to achieve good accuracy. A MATLAB program to find data on the tongues (of the HH system—it can be easily modified for HR) is included in Appendix C. XPP was not used to trace out the boundaries for the HR equations because of numerical issues that were encountered. The problem was most likely that these sets of equations are too stiff for XPP to handle (because of the action potentials).

The analytical phase-locking boundary for the SNIPER PRC given by Equation (3.23) can be written as

$$\frac{\omega}{\omega_f} - 1 = \pm \frac{I_f c_{sn}}{2\omega\omega_f C}. \tag{4.1}$$

Solving for I_f as a function of ω_f,

$$I_f = \mp \frac{2\omega C}{c_{sn}}(\omega - \omega_f). \tag{4.2}$$

Letting

$$\beta = \frac{I_f}{2\omega\omega_f C}, \tag{4.3}$$

Equation (4.2) simplifies to

$$\beta = \frac{1}{c_{sn}} \left(\frac{1}{\lambda} - 1 \right). \tag{4.4}$$

Note that data points found experimentally describing the phase-locking boundary

of a system can be expressed in terms of λ and β (because all terms are known). Fitting to Equation (4.4) will yield a value for c_{sn}.

The data from smaller I_f values that appeared to fall on a straight line was put into Mathematica and fit to Equation (4.4). Only this linear data was used because when plotted in dimensional terms (as the raw data is naturally, e.g. in Figure 4.1), the averaged solution to the phase-locking boundary consists of one linear segment on each side of the wedge (see Equation (4.2), Figures 2.7 and 3.4). Thus, not all the data was used for the fit, but all of the data was put into the plots. Figure 4.1 shows the results for finding a different value of c_{sn} for each value of I_b and plotting the boundaries (each one non-dimensionalized with the corresponding value of c_{sn}) all together. These fitted c_{sn} values can be used to draw the general shape of the phase response curves as shown in Figure 4.2. These are compared with the actual PRC of the Hindmarsh-Rose equations obtained numerically through XPP and a $(1 - \cos\theta)$ curve with a simple least-squares magnitude fit to the actual PRC. It also shows the three actual PRCs and a $(1 - \cos\theta)$ curve multiplied by c_{sn} fit from all of the data. Because $Z(\theta) \sim 1/\omega$, these curves are multiplied by ω so that the data (roughly) collapse to a single curve [5]. These results show that this method captures the general shape as well as the magnitude of the PRC with less than 6% error (the largest error being for the case $I_b = 5.10$, the test current farthest away from the bifurcation, and thus expected to have the largest error because the PRC looks less like $(1 - \cos\theta)$,

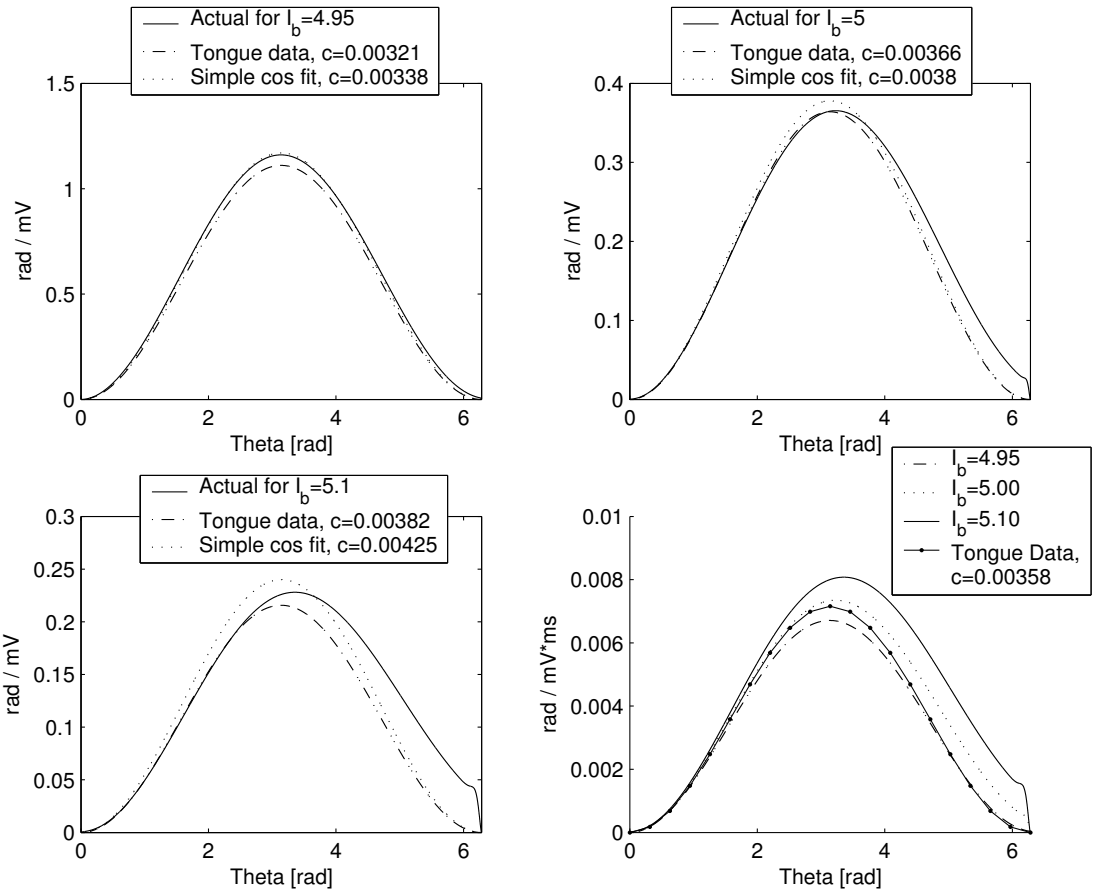

Figure 4.2: Phase response curves for HR data from three different I_b values. The curves in the bottom-right panel are multiplied by ω to remove the expected ω dependence of the magnitude of the PRCs.

instead having a larger contribution from higher-order Fourier terms). Also note that, as expected, the curves from the tongue data are always slightly smaller in magnitude than the actual PRCs. This is because they do not take into account the (small) contribution from the higher-order Fourier modes.

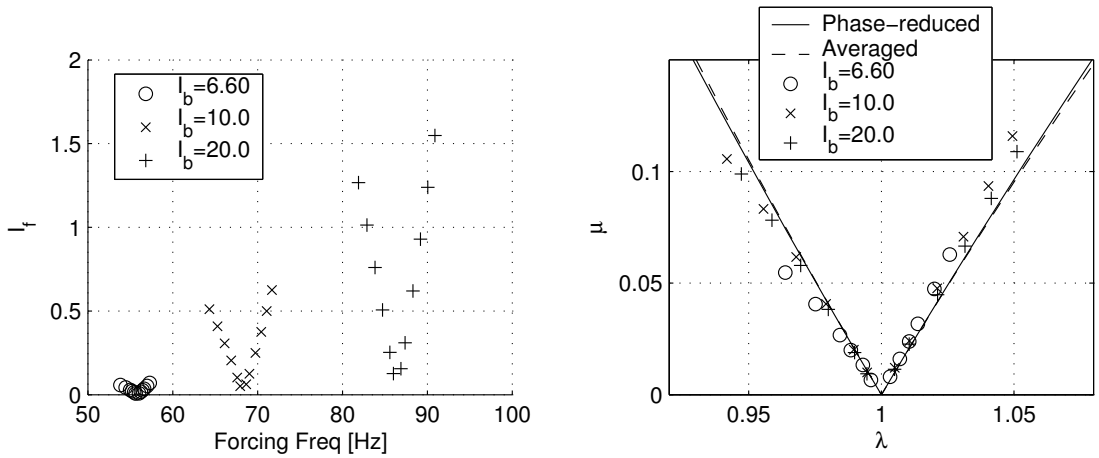

Figure 4.3: Left panel: Raw data taken for the phase-locking boundary of the HH system for three values of I_b. Right panel: Same data non-dimensionalized using c_B and ω_{SN} fitted to the Bautin averaged solution using data from all three I_b values.

4.3 Bautin PRC / Type II

Now suppose that a given neuron is of Type II (i.e. the value of the PRC changes from negative to positive). We assume that such a system can be described as having a Bautin bifurcation to periodicity. Numerical data for the 1:1 phase-locking boundary was taken for the HH equations, a Type II neuron model. The data, taken for three different values of the baseline current (I_b = 6.6, 10.0, 20.0), are shown in Figure 4.3.

As with HR in the previous section, a stroboscopic Poincaré map was made with MATLAB to find the phase-locking tongues for HH. When near the boundaries, it took an especially long time to determine if the system was locked with good accuracy, usually up to 1250 forcing cycles.

Rewriting the phase-locking boundary of the averaged system (Equation (3.23))

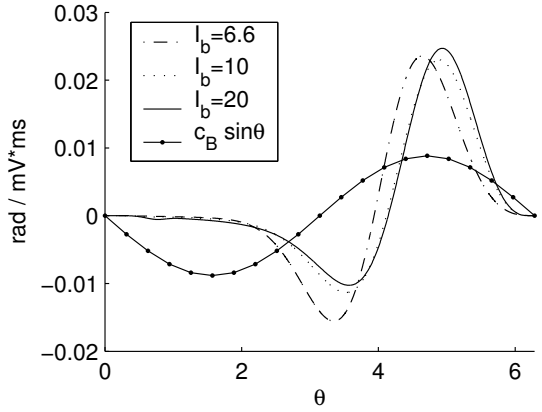

Figure 4.4: Phase response curves for HH data from three different I_b values. The actual PRCs are multiplied by $(\omega - \omega_{SN})$ to remove the expected $(\omega - \omega_{SN})$ dependence of the magnitude [5].

gives

$$\frac{\omega}{\omega_f} = 1 \pm \frac{I_f |c_B|}{2\omega_f |\omega - \omega_{SN}| C}. \tag{4.5}$$

In this case, the equation must be set up to do a two parameter fit to determine both c_B and ω_{SN}. Using λ and β as before simplifies Equation (4.5) to

$$\beta = \frac{|\omega - \omega_{SN}|}{\omega |c_B|} \left(\frac{1}{\lambda} - 1 \right). \tag{4.6}$$

Figure 4.3 also shows the results of fitting a value of ω_{SN} and c_B to all of the HH data and plotting them together using non-dimensionalized variables. For the HH model, parameter fits cannot be made for single I_b values as with the HR model because the fit to Equation (4.6) needs data from more than one I_b value to avoid being underdetermined. Thus, the only fit done used all of the data with the appropriate forcing strengths. Figure 4.4 shows the phase response curves for the different I_b values for the HH model, along with a $\sin\theta$ curve with amplitude c_B. Table 4.1 compares the actual and predicted values of the coefficients of the

Table 4.1: Comparison of actual and predicted Fourier terms for the HH system with $I_b = 10$.

I_b	$\sqrt{(a_1^{PRC})^2 + (b_1^{PRC})^2}$	$\frac{\lvert c_B \rvert}{\lvert \omega - \omega_{SN} \rvert}$	% Error
6.6	0.320	0.322	0.6
10.0	0.0793	0.0835	5.4
20.0	0.0399	0.0402	0.7

first Fourier terms. This shows that the 1:1 phase-locking tongue can be used to accurately predict the combination of the first terms in the Fourier decomposition of the PRC.

The lowest value of the injected current which maintained periodic firing in the HH system was $I_b = 6.269$, corresponding to $\omega_{SN} = 0.317$. The value from the fit was $\omega_{SN} = 0.324$, which is a 2.2% error.

One might suspect that using phase-locking data from the 2:1 and 3:1 tongues (and so on) would allow for a more accurate representation of the PRC to be put together, but this procedure only gives the quantity $\sqrt{a_j^2 + b_j^2}$, not the individual a_j and b_j values, meaning no phase information about the Fourier terms is available, and thus a PRC with more Fourier terms cannot be formed. However, knowing the quantity $\sqrt{a_j^2 + b_j^2}$ does allow for constraints to be formed for use with procedures to find PRCs from experimental data recently proposed in [9, 15]. These procedures use least-squares fits to individual Fourier terms, so knowing the relationships between some of the terms could lead to better results.

Chapter 5

Deducing neuron type from phase-locking data

5.1 Introduction

The phase-locking data can also be used to determine the type of neuron being studied (and thus which bifurcation gives rise to its periodicity). Here, models for Type I (HR) and Type II (HH) neurons have their underlying bifurcation determined from phase-locking data alone. This is accomplished by finding the best fit for the data using both SNIPER and Bautin universal entrainment curves and choosing the more likely one as the one which minimizes the variance of the fit while still suggesting parameters which are physically allowed.

Table 5.1: Parameter results from fitting HH and HR phase-locking data to the SNIPER and Bautin universal entrainment curves.

		HR	HH
SNIPER	c_{sn}	**0.00358**	0.0305
	σ^2	**0.554**	0.146
Bautin	c_B	0.00393	**0.00883**
	ω_{SN}	-0.00133	**0.324**
	σ^2	0.182	**0.0159**

5.2 Hindmarsh-Rose system

The non-dimensionalized data from the HR system fit to the SNIPER and Bautin universal entrainment curves (Equations (4.4) and (4.6)) are shown in Figure 5.1. Table 5.1 shows the numerical results of the fitting process. σ^2 is the variance as estimated by Mathematica. Both fits look good, but the key is that for the Bautin fit, ω_{SN} is negative, which has no physical meaning. If ω_{SN} is constrained to be non-negative, $\omega_{SN} = 0$ is the best fit, which yields the same result as the SNIPER case (and when plotted on the Bautin universal entrainment curve is clearly not an optimal fit judging visually, not shown). Thus, SNIPER must be the bifurcation displayed by the HR equations. Additionally, note how the HR data matches the SNIPER universal entrainment curve for very high values of μ, much higher than the values up to $\mu = 0.1$ used in the fits. Again, it was not necessary to know ahead of time any specific information about these equations or the type of neuron they represent.

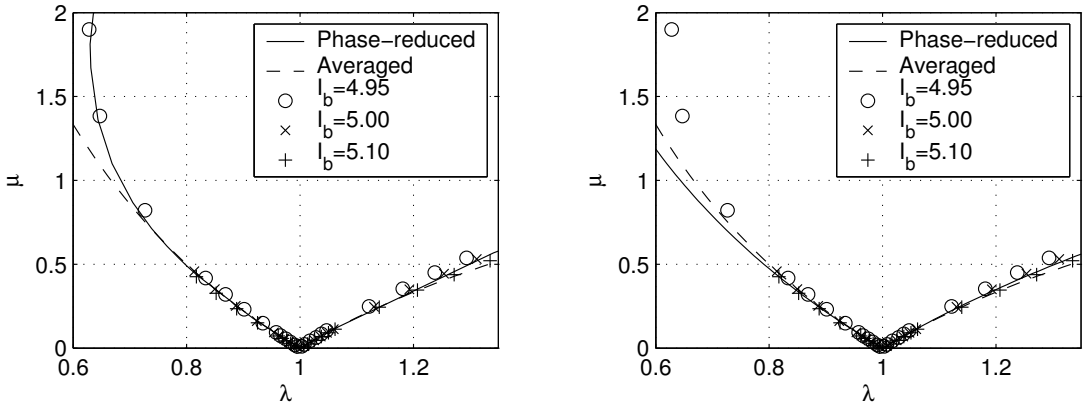

Figure 5.1: Left panel: Data from the HR system fit to the SNIPER universal entrainment curve. Right panel: Data from the HR system fit to the Bautin universal entrainment curve. The HR system has a SNIPER bifurcation.

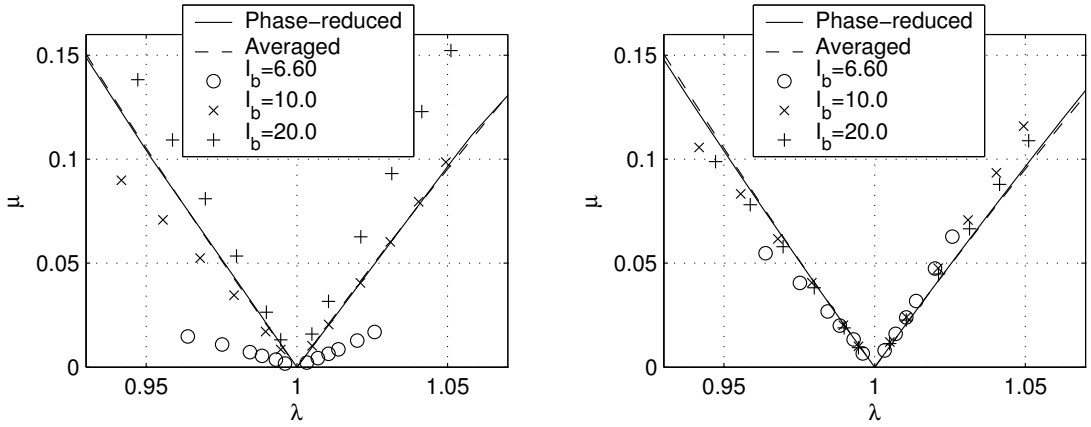

Figure 5.2: Left panel: Data from the HH system fit to the SNIPER universal entrainment curve. Right panel: Data from the HH system fit to the Bautin universal entrainment curve. The HH system can be described as having a Bautin bifurcation.

5.3 Hodgkin-Huxley system

The non-dimensionalized data from the HH system fit to both the SNIPER and Bautin universal entrainment curves is shown in Figure 5.2. Again, Table 5.1 shows the results of the parameters in the fitting process. In this case, it can be clearly seen by eye that the Bautin fit is better than the SNIPER fit. Both fits have physically possible parameters, but the statistical variance (9 times higher for the SNIPER fit) confirms a significant difference, leading to the conclusion that periodicity in HH neurons is best associated with a Bautin bifurcation, so that it is a Type II neuron.

5.4 Process for determining bifurcation type

With a set of data representing the 1:1 phase-locking boundary of a neuron, the underlying bifurcation type can be determined. A quick method to narrow down the choices of bifurcations can be used as a cross check of the more thorough method. As shown in Figure 2.6, due to the nature of the bifurcations, SNIPER and homoclinic neurons can fire arbitrarily slowly as I_b is reduced to be near the bifurcation. Bautin neurons do not have a stable periodic orbit that continuously shrinks into a fixed point, and cannot fire arbitrarily slowly. Hopf neurons have a periodic orbit that grows continuously from the fixed point, but the frequency is typically bounded away from zero. Due to the uncommonness of Hopf neurons,

it follows that if a neuron in the lab cannot fire arbitrarily slowly it is most likely Type II (Bautin PRC). Because homoclinic neurons are also uncommon, if a neuron can fire arbitrarily slowly, it is most likely Type I (SNIPER PRC).

More details on determining the bifurcation type occurring in a neuron are described in Appendix B.2.

Chapter 6

Conclusions and future work

Knowledge of how neurons respond to different types of stimuli could lead to better treatments of Parkinson's disease through therapies such as deep brain stimulation. Such response is characterized by the neuron's PRC, which is typically difficult to measure experimentally. This thesis has shown how properties of the PRC can be determined by considering the effects of sinusoidal stimuli on a neuron. Specifically, it has shown the relationships between the PRC of a neural oscillator and its phase-locking regions. Knowledge of the PRC can be used to generate good predictions for the whole-number ratio phase-locking tongue boundaries of an oscillator, and the phase-locking tongues can be used to get some information about the PRC. In the case of Type I neurons, data from the 1:1 Arnold tongue can lead to a very good approximation of the PRC. For Type II neurons, data from the tongues can be used to find combinations of the Fourier

coefficients of the PRC which can be used as constraints in fitting procedures that generate Fourier coefficients of the PRC from experimental data [9, 15]. For Type II neurons we can also give a good estimate of the minimum frequency at which periodic behavior will be observed. If it is known that a particular group of Type II neurons has a PRC that is close to sinusoidal in nature, our procedure can give a good approximation of the magnitude of the PRC.

It was shown that the phase-reduced version of an oscillator has dynamics very similar to the full system it represents. This is what allows for the bifurcation type of an unknown neuron to be determined—normal form theory says that systems with each of the codimension one bifurcations to periodicity have a different form of the PRC. The dynamics of the full neural systems are similar enough to the phase-reduced systems with PRCs from the normal forms of the bifurcations that they can be associated with one another for identification. Determining the neuron type does not require any previous knowledge about the neural system.

If there was a way to generate information about the phases of a PRC's Fourier components generated by our method, then it could be possible to take data from several whole-number ratio tongues and synthesize the PRC with as many Fourier terms as needed. Another possible extension of our method would be to take a Fourier decomposition of an arbitrary periodic current stimulus, $I_f(t)$, and use information about responses to sinusoidal forcing to determine the response of the system to this arbitrary input.

This work will also provide insights into the dynamics of populations of oscillators with randomly distributed initial phases subjected to sinusoidal forcing. This will allow one to see how quickly a group of oscillators can be synchronized or desynchronized and if there are any special distributions the neurons take on. In future work, periodically forced population models could include coupling, noise, or different distributions of the individual oscillators' natural frequencies.

Finally, the work done in this thesis can be applied to more models such as those for circadian rhythms or the types of neurons involved in Parkinson's disease to find out what can be said about the response dynamics of these systems. Eventually, a closed-loop control systems problem could be formulated for the deep brain stimulation treatment instead of the current open-loop approach that would desynchronize the neurons using a more optimal, likely lower-power method. A similar problem could be devised for circadian rhythms, where a control system could apply light to a user in such a way as to avoid jet lag. Additionally, an input shaped more like the way the sun works could be fed into a circadian system by creating it with terms from a Fourier series, to which this thesis provides information about the response.

Bibliography

[1] P. Bak. The Devil's staircase. *Physics Today*, 39:38–45, December 1986.

[2] A. L. Benabid, P. Pollak, C. Gervason, D. Hoffmann, D. M. Gao, M. Hommel, J. E. Perret, and J. De Rougemont. Long-term suppression of tremor by chronic stimulation of the ventral intermediate thalamic nucleus. *The Lancet*, 337:403–406, 1991.

[3] S. Blond, D. Caparros-Lefebvre, F. Parker, R. Assaker, H. Petit, J.-D. Guieu, and J.-L. Christiaens. Control of tremor and involuntary movement disorders by chronic stereotactic stimulation of the ventral intermediate thalamic nucleus. *J. Neurosurg.*, 77:62–68, 1992.

[4] E. Brown, P. Holmes, and J. Moehlis. Globally coupled oscillator networks. In E. Kaplan, J. Marsden, and K.R. Sreenivasan, editors, *Perspectives and Problems in Nonlinear Science: A Celebratory Volume in Honor of Larry Sirovich*, pages 183–215. Springer-Verlag, New York, 2003.

[5] E. Brown, J. Moehlis, and P. Holmes. On the phase reduction and response dynamics of neural oscillator populations. *Neural Comp.*, 16:673–715, 2004.

[6] E. Brown, J. Moehlis, P. Holmes, E. Clayton, J. Rajkowski, and G. Aston-Jones. The influence of spike rate and stimulus duration on noradrenergic neurons. *J. Comp. Neuroscience*, 17:13–29, 2004.

[7] J. Cronin. *Mathematical aspects of Hodgkin-Huxley neural theory.* Cambridge University Press, Cambridge, 1987.

[8] G. B. Ermentrout. *Simulating, Analyzing, and Animating Dynamical Systems: A Guide to XPPAUT for Researchers and Students.* SIAM, Philadelphia, 2002.

[9] R. F. Galan, G. B. Ermentrout, and N. N. Urban. Efficient estimation of phase-resetting curves in real neurons and its significance for neural-network modeling. *Phys. Rev. Lett.*, 94:158101, 2005.

[10] L. Glass. Synchronization and rhythmic processes in physiology. *Nature*, 410:277–284, 2001.

[11] J. Guckenheimer. Isochrons and phaseless sets. *J. Math. Biol.*, 1:259–273, 1975.

[12] J. Guckenheimer and P. J. Holmes. *Nonlinear Oscillations, Dynamical Systems and Bifurcations of Vector Fields.* Springer-Verlag, New York, 1983.

[13] B. S. Gutkin, G. B. Ermentrout, and A. D. Reyes. Phase response curves give the responses of neurons to transient inputs. *J. Neurophysiol.*, 94:1623–1635, 2005.

[14] A. L. Hodgkin and A. F. Huxley. A quantitative description of membrane current and its application to conduction and excitation in nerve. *J. Physiol.*, 117:500–544, 1952.

[15] E. M. Izhikevich. *Dynamical Systems in Neuroscience: The Geometry of Excitability and Bursting*. Springer, New York, 2005. To be published.

[16] D. Johnston and S. M.-S. Wu. *Foundations of Cellular Neurophysiology*. MIT Press, Cambridge, MA, 1995.

[17] J. Keener and J. Sneyd. *Mathematical Physiology*. Springer, New York, 1998.

[18] M. P. Kennedy, K. R. Krieg, and L. O. Chua. The Devil's staircase: The electrical engineer's fractal. *IEEE Trans Circuits Syst*, 36:1133–1139, 1989.

[19] J. C. Lagarias and C. P. Tresser. A walk along the branches of the extended Farey tree. *IBM J. Res. Dev.*, 39(3):283–294, 1995.

[20] B. B. Mandelbrot. *Fractals: Form, Chance, and Dimension*. Freeman, San Francisco, 1977.

[21] D. Pare, R. Curro'Dossi, and M. Steriade. Neuronal basis of the Parkinsonian

resting tremor: a hypothesis and its implications for treatment. *Neuroscience*, 35:217–226, 1990.

[22] A. Pikovsky, M. Rosenblum, and J. Kurths. *Synchronization: A Universal Concept in Nonlinear Sciences*. Cambridge University Press, Cambridge, 2001.

[23] J. Rinzel and R. N. Miller. Numerical calculations of stable and unstable periodic solutions to the Hodgkin-Huxley equations. *Math. Biosci.*, 49:27–59, 1980.

[24] R. Rose and J. Hindmarsh. The assembly of ionic currents in a thalamic neuron I. The three-dimensional model. *Proc. R. Soc. Lond. B*, 237:267–288, 1989.

[25] M. Smolensky. Chronobiology and chronotherapeutics: applications to cardiovascular medicine. In P. C. Deedwania, editor, *Circadian Rhythms of Cardiovascular Disorders*, pages 173–206. Futura, Armonk, NY, 1997.

[26] S. Strogatz. *Sync: The Emerging Science of Spontaneous Order*. Hyperion, New York, 2003.

[27] S. H. Strogatz. From Kuramoto to Crawford: exploring the onset of synchronization in populations of coupled oscillators. *Physica D*, 143:1–20, 2000.

[28] P. A. Tass. *Phase Resetting in Medicine and Biology.* Springer, New York, 1999.

[29] P. A. Tass. Synergetics of the nervous system: from basic principles to therapy. *Nonlin. Phenom. Complex Syst.*, 5:470–478, 2002.

[30] S. Wiggins. *Introduction to Applied Nonlinear Dynamical Systems and Chaos, Second Edition.* Springer, New York, 2003.

[31] A. Winfree. Patterns of phase compromise in biological cycles. *J. Math. Biol.*, 1:73–95, 1974.

[32] A. Winfree. *The Geometry of Biological Time, Second Edition.* Springer, New York, 2001.

Appendix A

Equations for the neural models

Included below are equations for the two neural models discussed in detail in this thesis. To add sinusoidal forcing to either one, replace I_b with $I_b + I_f \sin(\omega_f t)$.

The Hindmarsh-Rose equations:

$$\begin{aligned}
\dot{V} &= [I_b - g_{Na} m_\infty(V)^3(-3(q - Bb_\infty(V)) + 0.85)(V - V_{Na}) \\
&\quad -g_K q(V - V_K) - g_L(V - V_L)]/C \\
\dot{q} &= (q_\infty(V) - q)/\tau_q(V) \\
q_\infty(V) &= n_\infty(V)^4 + Bb_\infty(V)\ , \quad b_\infty(V) = (1/(1 + \exp(\gamma_b(V + 53.3))))^4\ , \\
m_\infty(V) &= \alpha_m(V)/(\alpha_m(V) + \beta_m(V))\ , \quad n_\infty(V) = \alpha_n(V)/(\alpha_n(V) + \beta_n(V))\ , \\
\tau_q(V) &= (\tau_b(V) + \tau_n(V))/2\ , \quad \tau_n(V) = T_n/(\alpha_n(V) + \beta_n(V))\ , \\
\tau_b(V) &= T_b(1.24 + 2.678/(1 + \exp((V + 50)/16.027)))\ , \\
\alpha_n(V) &= 0.01(V + 45.7)/(1 - \exp(-(V + 45.7)/10))\ ,
\end{aligned}$$

$$\alpha_m(V) = 0.1(V+29.7)/(1-\exp(-(V+29.7)/10)) ,$$

$$\beta_n(V) = 0.125\exp(-(V+55.7)/80) , \quad \beta_m(V) = 4\exp(-(V+54.7)/18) .$$

Parameters:

$$I_b, I_f = [\mu\text{A/cm}^2] ,$$

$$V_{Na} = 55 \text{ mV} , \ V_K = -72 \text{ mV} , \ V_L = -17 \text{ mV} , \ g_{Na} = 120 \text{ mS/cm}^2 ,$$

$$g_K = 20 \text{ mS/cm}^2 , \ g_L = 0.3 \text{ mS/cm}^2 , \ g_A = 47.7 \text{ mS/cm}^2 ,$$

$$C = 1 \ \mu\text{F/cm}^2 , \ \gamma_b = 0.069 \text{ mV}^{-1} , \ T_b = 1 \text{ msec} ,$$

$$T_n = 0.52 \text{ msec} , \ B = 0.21 \, g_A/g_K.$$

The Hodgkin-Huxley equations:

These equations are written using modern conventions and look slightly different than those given in [14]. One obtains the equations in the paper by letting $V_{HH} = -V - 65$.

$$dV/dt = [I_b - g_{Na}h(V-V_{Na})m^3 - g_K(V-V_K)n^4 - g_L(V-V_L)]/C$$

$$dm/dt = a_m(V)(1-m) - b_m(V)m$$

$$dh/dt = a_h(V)(1-h) - b_h(V)h$$

$$dn/dt = a_n(V)(1-n) - b_n(V)n$$

$$a_m(V) = 0.1(V+40)/(1-\exp(-(V+40)/10))$$

$$b_m(V) = 4\exp(-(V+65)/18)$$

$$a_h(V) = 0.07\exp(-(V+65)/20)$$

$$
\begin{aligned}
b_h(V) &= 1/(1+\exp(-(V+35)/10)) \\
a_n(V) &= 0.01(V+55)/(1-\exp(-(V+55)/10)) \\
b_n(V) &= 0.125\exp(-(V+65)/80)
\end{aligned}
$$

Parameters:

$$I_b, I_f = [\mu\text{A/cm}^2] \ ,$$

$$V_{Na} = 50 \text{ mV} \ , \ Vk = -77 \text{ mV} \ , \ V_L = -54.4 \text{ mV} \ , \ g_{Na} = 120 \text{ mS/cm}^2$$

$$g_K = 36 \text{ mS/cm}^2 \ , \ g_L = .3 \text{ mS/cm}^2 \ , \ C = 1 \ \mu\text{F/cm}^2$$

Appendix B

Detailed process for determining PRC properties and neuron bifurcation types

B.1 Determining PRC properties

Details of the method used in this thesis for finding points on the phase-locking boundaries of the neural systems follows.

1. Get numerical data for 1:1 phase-locking boundaries of neurons

    - Use a range of baseline current values, I_b, to capture three significantly different natural frequencies, with one value of I_b being near the bifurcation

- Care must be taken for I_b values near the bifurcation—if I_f is too large, it may push the neuron to an I_b value below the bifurcation during part of the forcing cycle, yielding unpredictable results (recall that the total current injected into the system is $I_{tot} \sim I_b + I_f$)
- If data is inconsistent at higher I_f values, it may be because the neuron is not returning to the limit cycle fast enough while being forced—use smaller I_f values
- In this thesis, six data points at each I_b value were used to make a good fit
- Use the same number of data points for each value of I_b
- Using an initial guess for the needed parameters, try to limit μ, the non-dimensional forcing strength, to 0.1 or less (this is an order of magnitude figure for the region of linearity of the tongue boundary)
- After taking a set of data, examine if the portion of the boundary traced is linear. If it is, more data can (but not necessarily should) be taken at higher I_f values. If not, more data should be taken at lower I_f values.

2. Put the data into a spreadsheet to calculate the λ and β parameters for all data points to be fitted, as shown in Section 4.2. The triplet $\{\lambda, \omega, \beta\}$ will be fed to Mathematica. Again, only data that appears linear should be put

into Mathematica for the fit.

3. Use Mathematica to fit the data taken to the appropriate model

   - Run this code first to load the needed toolbox:

     `<< Statistics‘NonlinearFit‘`

   - Put the data into this format:

     `data={{`λ`, `ω`, `β`},...,{`λ`, `ω`, `β`}}`

     Data points with $\lambda > 1$ should be adjusted to have a negative β value due to the nature of the $(1/\lambda - 1)$ curve.

   - SNIPER fit command:

     `NonlinearRegress[data, (1/lambda - 1)/c, {x, w}, {c}]`

   - Bautin fit command:

     `NonlinearRegress[data, (w - wsn)(1/lambda - 1)/(w cB), {x,w},`
     `{{cB, .1}, {wsn, 0.1}}]`

     Note that running this fit requires data that includes more than one I_b value to prevent the problem from being underdetermined.

Running this code will yield values for the different parameters of the system along with many statistical results, the most important of which is the variance. These fitted parameters can be used to get a much better idea of the actual μ values tested than from the initial guess. Using this, confirm that the values used in the fit fall below about 0.1. Values above 0.1 are useful when plotting,

but the nonlinearity of the actual tongue boundaries begins to be more prevalent and reduces the accuracy of the resulting parameters. Also, the PRC, which was derived for small forcing, might begin to lose validity at higher forcing strengths.

B.2 Determining neuron bifurcation type

A more thorough method than described in Section 5.4 to determine the bifurcation type that takes advantage of the phase-locking data is as follows:

Case 1 Fit to Bautin universal entrainment curve is unreasonable / has high variance, SNIPER fit is reasonable / has low variance: System characterized by SNIPER

The Bautin fit may yield an unreasonable result, such as a negative value for ω_{SN}. This means that the best fit (with physically possible parameters) actually has $\omega_{SN} = 0$, which corresponds to the SNIPER case. It is important to note that if a fit gives parameters that are not physically possible, it cannot represent the proper bifurcation—this rule takes precedence over any involving variance.

Case 2 Fit to Bautin universal entrainment curve is reasonable / has low variance, SNIPER fit has high variance: System characterized by Bautin

In this case, when the data non-dimensionalized with the SNIPER c_{sn} are plotted, different linear trends for the data are clearly seen corresponding

to different values of I_b, as was observed in Figure 5.2. The data non-dimensionalized with the Bautin parameters fall more closely onto a single curve, giving the fit a much lower variance.

Appendix C

MATLAB program to find Arnold tongues

The following MATLAB program was used to find the data points on the 1:1 phase-locking boundary of the HH system. Varying the forcing frequency, it uses a binary search algorithm at a given forcing strength to check if the system is entrained to the forcing at that point. A plot is generated for every point the program checks so that the algorithm can be confirmed visually.

The program can easily be changed to find data for other neural models, and can also be modified to find data at 2:1 and higher tongues. With the exception of the forcing term, the code for the HH system contained in the `odefunc` function and below is generic.

```
---------- syncfinderHHauto.m ----------
% works with one I_b value at a time - change I_b (I) in odefunc
% Primary inputs: I, freqnat, lambda, numCycles, cB, wsn, mu
```

```
function syncfinderHHauto
global omegaf forceAmp;
tic
freqnat=68.3;  % entered manually - really only sets inital lower value
omegan = (freqnat*2*pi)/1000;

lambda=1.1; % initial guess - sets 'upper' value.
% Greater than 1 gets points on right, less than 1 gets points on left

freqforce=freqnat*lambda;
omegaf = (freqforce*2*pi)/1000; % max omegaf, used for mu approximation
numCycles=1250;

cB=0.009;  % guess of c value to get forceAmp from mu's fairly correct
wsn=0.310;  % guess of omega_{saddle node}
mu = [0.01 0.02 0.04 0.06 0.08 0.10];  % desired mu locations to search

forceAmpArray = mu*omegaf*(omegan-wsn)/cB; % array of I_f values

for i=1:length(forceAmpArray) % loop through I_f values
    forceAmp=forceAmpArray(i);
    lower=freqnat;
    upper=freqnat*lambda;
    synced = 0;

    while abs(upper-lower) > 0.005
    % loop until boundary is enclosed by two values close to each other
        mid = (lower+upper)/2;
        synced = hhsim(numCycles,mid);  % forceAmp sent via a global var
        if synced
            lower=mid;
        else
            upper=mid;
        end
    end

    mu_i = mu(i) % print out the results
    forceAmp
    freqforce = lower % outputs point closest to tongue that still locks
end
elapsed_hours=toc/3600  % takes a while to run this code

function synced = hhsim(numCycles,freqforce)
global omegaf forceAmp;
```

```
omegaf = (freqforce*2*pi)/1000;
cycleTime = 1000/freqforce;
TFINAL=numCycles*1000/freqforce;
IC = [-74.95951612406819   0.63292036803569   0.01543265525027 ...
      0.18523851622145];

points(1)=IC(1); % voltage is first state-variable
counter=2;
for i=0:cycleTime:TFINAL
    [t,x] = ode23s(@odefunc,[i i+cycleTime],IC);
    IC=x(length(x),:);
    points(counter)=IC(1);
    counter=counter+1;
end

figure  % make and label plot
plot(points,'.-')
xlim([1 numCycles+2])
title(['freqforce=' num2str(freqforce) '  forceAmp=' num2str(forceAmp)])

% synced?  check second half of points for small enough voltage diff
points=points(length(points)/2:length(points));
deltav=abs(max(points)-min(points));
if deltav < 0.5
    synced = 1;
else synced = 0;
end

function ydot=odefunc(t,y)
global omegaf forceAmp
gna = 120; % mmho/cm^2    % constants
gk = 36; % mmho/cm^2
gl = 0.3; % mmho/cm^2
Vna = 50; % mV
Vk = -77; % mV
Vl = -54.4; % mV
C = 1; % microF/cm^2
I = 10; % microA/cm^2 - Entered manually here!

ydot=[(I-gna*y(3)^3*y(4)*(y(1)-Vna)-gk*y(2)^4*(y(1)-Vk)-gl*(y(1)-Vl)+...
      forceAmp*sin(omegaf*t))/C
    alpha_n(y(1))*(1-y(2))-beta_n(y(1))*y(2)
    alpha_m(y(1))*(1-y(3))-beta_m(y(1))*y(3)
    alpha_h(y(1))*(1-y(4))-beta_h(y(1))*y(4)];
```

```
function val=alpha_n(V)
val = 0.01*(V+55)/(1-exp(-(V+55)/10));
function val=alpha_m(V)
val = 0.1*(V+40)/(1-exp(-(V+40)/10));
function val=alpha_h(V)
val = 0.07*exp(-(V+65)/20);
function val=beta_n(V)
val = 0.125*exp(-(V+65)/80);
function val=beta_m(V)
val = 4*exp(-(V+65)/18);
function val=beta_h(V)
val = 1/(1+exp(-(V+35)/10));
```